

# Antagonistic Series Elastic Actuation for a Variable Stiffness Robotic Endoscope

Lorin Fasel <sup>ID</sup>, Nicolas Gerig <sup>ID</sup>, Member, IEEE, Aschraf Danun <sup>ID</sup>, Mirko Meboldt <sup>ID</sup>, Raphael Guzman, Philippe C. Cattin <sup>ID</sup>, and Georg Rauter <sup>ID</sup>, Member, IEEE

**Abstract**—Minimally invasive neuroendoscopic procedures through the ventricular system are common to treat intraventricular pathologies. However, current rigid tools lack the maneuverability to safely access the entire ventricles. Robotic joints at the tip of the endoscope could resolve this, but unintended contacts with the brain tissue pose a safety threat. Here, we propose a bio-inspired joint actuation concept for a tendon-driven robotic endoscope for minimally invasive (neuro-)surgery. Drawing inspiration from the human musculoskeletal system, we incorporated antagonistic series elastic actuators (SEAs) to drive discrete endoscope joints. Our approach leverages the advantages of SEAs, such as mechanical compliance, faster reaction to impacts, and robust torque control. Endoscope joint stiffness can be varied during operation by continuously varying the pretension on the nonlinear springs of the actuation. We found that our prototype with two distal joints would be suitable for the expected position control maneuvers of such a neuroendoscope. Further, joint torque could be estimated with errors in the milli-Newton-meter range, deemed sufficient for detecting harmful forces. The compliant actuation absorbed external impacts, and the rise of contact forces was slower when the pretension on antagonistic tendons was decreased. While the spring design procedure needs improvement to account for friction and other transmission nonlinearities, our actuation concept holds promise for force control of tendon-driven joints. Specifically, its use in neurosurgery could provide

the surgeon with increased maneuverability while ensuring a safe operation.

**Index Terms**—Bio-inspired, minimally invasive surgery, robotic neuro-surgery, variable impedance actuators.

## I. INTRODUCTION

BRAIN surgery carries the risk of severe neurological deficits if sensitive structures are injured. To minimize damage, neurosurgical interventions are increasingly performed with minimally invasive techniques, such as intraventricular neuroendoscopy [1]. This procedure involves endoscopic inspection and treatment of pathologies in or near the ventricular system—a cavity system filled by the cerebrospinal fluid, embedded within the brain tissue [2]. Using preoperative imaging and computer-assisted navigation, surgeons can reach the ventricles typically with a rigid endoscope with limited damage to surrounding brain regions [3]. The endoscope contains the optics to visually inspect the site. Through the working channel, tools can be inserted to take biopsies or manipulate and remove tissue. One common neuroendoscopic procedure is the endoscopic third ventriculostomy [4], which relieves intraventricular pressure by fenestrating the floor of the third ventricle in situations of hydrocephalus [see Fig. 1(a)]. The cause of the pressure increase can be manyfold, but it is sometimes an obstruction of the fluid circulation in the posterior part of the third ventricle, for example, due to a tumor. Therefore, it can be necessary to reach and inspect the posterior part of the third ventricle during the intervention to take biopsies, remove a mass, or stent the opening to the fourth ventricle. [5]. Moving or tilting the rigid shaft in order to reach the posterior third ventricle (or other parts of the ventricular system) can injure critical anatomical structures surrounding the third ventricle [6], thus creating the need for additional degrees of freedom at the endoscope tip.

Robotically controlling the additional degrees of freedom of the endoscope [see Fig. 1(b)] is promising to make endoscope steering more intuitive, reduce the cognitive workload, and increase patient and device safety. Previously developed robotic systems to provide additional degrees of freedom in neuroendoscopy include concentric tube robots [7], [8], cable-driven continuum robots [9], or wristed robotic instruments [10]. A typical robotic surgery system consists of a remote-controlled patient-side robot (“telemanipulated”) by the surgeon sitting at a console. Thus, the surgical instruments are mechanically decoupled from the surgeon’s hands. On one side, this

Received 4 March 2024; revised 3 July 2024; accepted 3 October 2024. Recommended by Technical Editor M. Liarokapis and Senior Editor Y.-J. Pan. This work was supported in part by Werner Siemens Foundation, Zug, Switzerland, by the Swiss National Centre of Competence in Research in Robotics (NCCR Robotics), and by Eucor-The European Campus, in part by the Werner Siemens Foundation through Project MIRACLE & MIRACLE-2, in part by Swiss National Science Foundation through NCCR Robotics under Grant 185543, in part by the Spin Fund through project name: “Variable Stiffness SEA-Scope: Safe Human-Machine Interaction in Neurosurgery,” and in part by the Eucor-The European Campus through the Seed Money project “Eye of the surgeon.” (Corresponding author: Nicolas Gerig.)

Lorin Fasel, Nicolas Gerig, Philippe C. Cattin, and Georg Rauter are with the Department of Biomedical Engineering, University of Basel, 4123 Allschwil, Switzerland (e-mail: lorin.fasel@unibas.ch; nicolas.gerig@unibas.ch).

Aschraf Danun and Mirko Meboldt are with Product Development Group Zurich pdz, ETH Zürich, 8092 Zürich, Switzerland.

Raphael Guzman is with the Department of Biomedical Engineering, University of Basel, 4123 Basel, Switzerland, and also with the Department of Neurosurgery, University Hospital Basel, 4031 Basel, Switzerland.

This article has supplementary material provided by the authors and color versions of one or more figures available at <https://doi.org/10.1109/TMECH.2024.3484583>.

Digital Object Identifier 10.1109/TMECH.2024.3484583

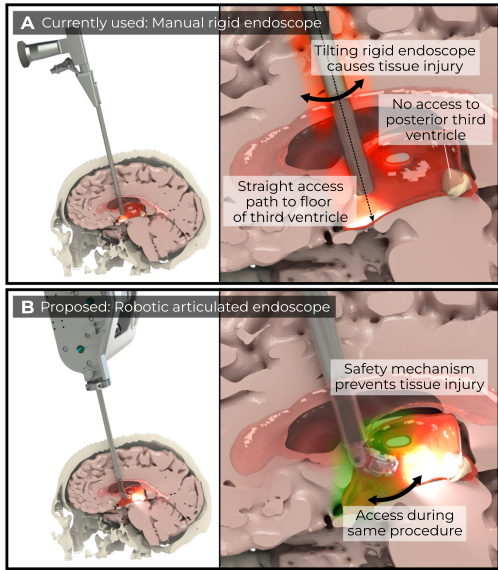


**Fig. 1.** Intraventricular endoscopy using (a) manual rigid endoscope versus and (b) robotic articulated endoscope.

decoupling opens the possibility of scaling motion and filtering out unwanted tremors, but on the other side, surgeons lose the haptic perception of their instruments interacting with tissue. They only “see” but do not “feel” the interaction. Haptic feedback has been identified as an important requirement for surgical robots [11], [12], since a lack thereof can lead to less intuitive control, loss of functionality (e.g., not being able to characterize tissue stiffness [13]), and in the worst case lead to safety issues. For example, high interaction forces between the instrument and the tissue cannot be detected if they happen outside the field of view of the endoscopic camera [14]. Therefore, a safety mechanism for robotically controlled endoscopes that prevents injury to brain tissue while performing the surgery is needed.

Existing approaches for safety mechanisms of robotic endoscopes employ sensors at the endoscope tip [15], [16] and a control strategy to react to conditions like exceeding force thresholds [17]. However, placing additional components in the endoscope tip limits the miniaturization and sterilization capabilities of the device [18]. Robotic instruments for minimally invasive surgery are often actuated extrinsically, i.e., the motors are placed in a part that stays outside the body during surgery, and the motion is transmitted to the instruments’ tip through a tendon mechanism. Instead of trying to measure the forces at the tip, measuring forces further back in the motion transmission could help to estimate forces or torques at the instrument tip [19]—at the cost of errors due to tendon friction and elasticity [18]. Estimating motor torque and instrument tip contact forces from the motor current can be noise-prone and requires filtering [20]. Another approach to receive contact force information is to measure the tension on the tendons with load cells [21] or by using an elasticity model of the tendons themselves [22]. However, one problem persists with most safety mechanisms based on software control: the safety function will react only once harmful forces are measured. Therefore, injuries might have already occurred before the safety function is activated.

To avoid damage before a time-discrete safety control can react, we deliberately include elastic elements into the transmission, which help absorb the energy from collisions between the instrument tip and the tissue and slow down the rise of forces at impact. Such an intrinsic safety mechanism based on mechanical, passive compliance reacts faster than any control loop [23]. The elastic element is inserted between the motor and the load (i.e., the movable degrees of freedom at the tip). This configuration is known as series elastic actuation (SEA) [24] and has been employed in different fields of robotics, such as legged robots [25] or robotic exoskeletons [26], [27]. Our preliminary results suggest it could be useful for an articulated robotic system used in minimally invasive surgery [28], [29], [30]. In addition to their impact absorption capabilities, the elastic elements can be used to estimate the force/torque exerted on them by measuring their deflection [24]. This deflection measurement can be realized with deterministic position sensors, which enable accurate and stable force control at the output [24], [31].

Choosing the stiffness, or more generally, the impedance of the elastic element in SEA, is a tunable tradeoff: softer elements absorb more impact energy and provide better force measurement sensitivity, but they also limit the achievable control bandwidth. One way to extend SEA capabilities is to vary the stiffness of the elastic elements [32]. For example, the stiffness could be decreased to absorb impacts while repositioning the endoscope camera, but it could be increased to provide precise motion control during insertion. This mechanical variation in joint stiffness is inspired by the musculoskeletal system, where the central nervous system varies joint stiffness in two ways to adapt to specific tasks or environments [33], [34]: 1) modulating joint stiffness by co-contracting antagonistic muscles and 2) actively controlling joint stiffness using negative position feedback. The human finger, for example, is stiffened by the coactivation of flexor and extensor muscles in the forearm during fast movements to improve motion control [35] or to hold its position in the presence of external disturbances [36]. Conversely, the central nervous system also actively controls finger muscle activity in response to muscle stretch [37]. The same two methods for varying joint stiffness can be implemented in robotics, with the same respective limitations [33], [34]. Active feedback control (e.g., impedance control) is slower due to time discretization and transmission delays, while passive modulation with antagonistic actuators uses energy for cocontraction without performing actual mechanical work. There has been extensive research on variable stiffness actuators: reviews exist on the state-of-the-art [38], the design aspects [32], [39], and considerations for their use in an application [40], [41]. Variable stiffness actuators with discrete joints have mainly been employed in legged robots [42], rehabilitation robots [43], [44], or collaborative robots [45], but to the best of the authors’ knowledge, not in surgical robotics. For surgical applications, variable stiffness *continuum* devices and robots have been presented [46], [47], [48], [49]—without completely eliminating the disadvantages of continuum robots, i.e., their complexity in modeling, sensing, and control.

Therefore, in this article, we propose a bio-inspired actuation concept (see Section II-A) for tendon-driven robots used in minimally invasive surgery. By combining antagonistic

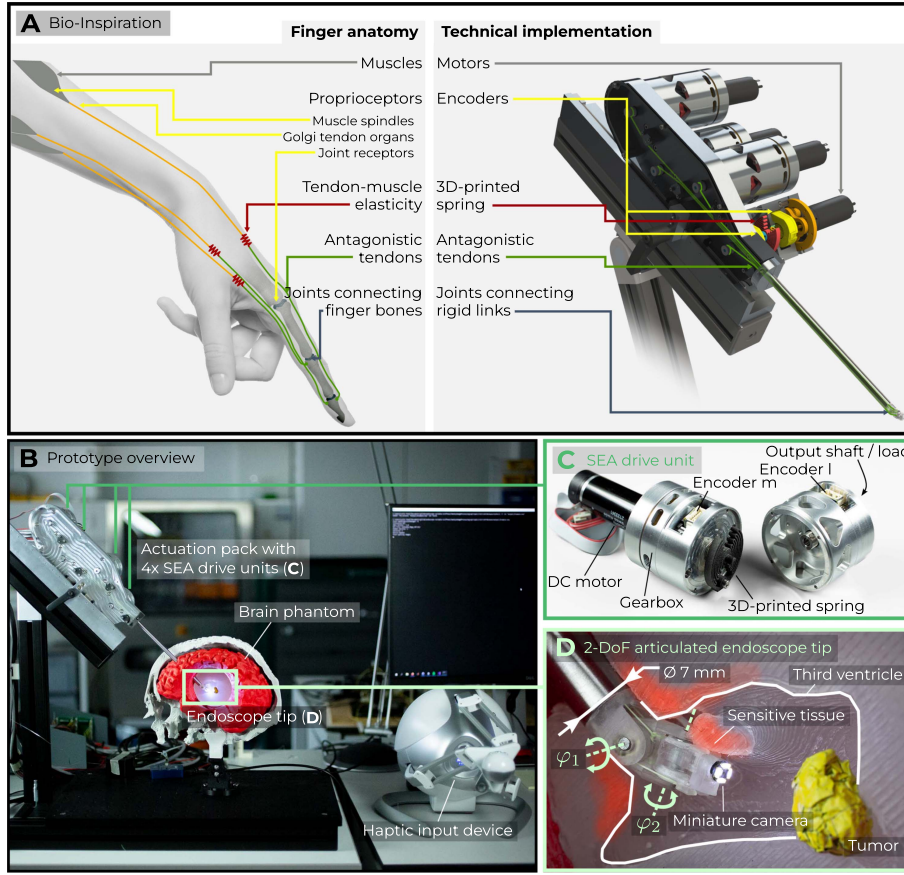


**Fig. 2.** (a) The actuation design of our robotic neuroendoscope (right) was inspired by the anatomy of a human finger (left). (b) Overview of the proposed prototype. The robot consisted of an endoscopic part, which was remotely driven via tendons by an actuation pack that consisted of four identical drive units. (c) Each drive unit was built based on the concept of series elastic actuation, i.e., an elastic element in the form of a 3D-printed nonlinear spring was integrated in series between the dc motor/gearbox and the load. Rotational absolute encoders were placed on the motor side (Encoder m) of the spring and on the load side (Encoder l) to measure the deflection of the spring. The output shaft of the drive units was connected to the links of an articulated endoscope tip via tendons. (d) This endoscope tip had two degrees of freedom to allow inspection of the third ventricle with a miniature camera.

series elastic actuation with discrete joints, we expect the following advantages: having (i) a reliable and accurate kinematic model and knowledge of the robot shape while at the same time (ii) providing mechanical compliance and (iii) enabling robust force/torque sensing and (iv) control. We test (i) with a forward kinematic model evaluation experiment (see Section II-C1), (ii) with an experiment evaluating the system's response to an external impact (see Section II-C4), (iii) by evaluating the joint torque estimation model (see Section II-C3), and (iv) by evaluating the system's response to high-level position control demands at different frequencies. Furthermore, we explore the potential to vary the stiffness of individual joints by repeating selected experiments at varying tendon pretensions.

## II. MATERIALS AND METHODS

### A. Bio-Inspired System Design

The endoscope tip joints were actuated antagonistically. The human finger anatomy served as a role model for the technical implementation of the robotic endoscope (see Fig. 2). Motors

(RE25 brushed dc motors, Maxon Motor AG, Sachseln, Switzerland) provided mechanical energy to pull on low-stretch fishing wire tendons (Berkley NanoFil, Pure Fishing, Inc., Columbia, SC, USA), mimicking flexor and extensor digitorum muscles in our forearms pulling on biological tendons. The fishing wire tendons were routed through the endoscope (corresponding to the forearm in the case of finger actuation). On the distal end, the tendons were fixed to rigid links, moving around rotational joints. These rigid links corresponded to the phalanges, which are the bones constituting our fingers. Since the tendon was attached to the rigid link at a distance from the axis of rotation, pulling on a tendon resulted in a torque around the endoscope joint. Tendons can only be used for motion transmission in the pulling direction, requiring two motor-tendon drive trains for independent control of agonist and antagonist tendons. Pulling the agonist tendon resulted in a positive torque, while pulling the antagonist tendon resulted in a negative torque. While the design of the endoscope links would allow  $\pm 90^\circ$  joint angles, we restricted the maximal joint angle to  $\pm 40^\circ$  in the control since the tendons slid out of their designated grooves at larger angles.

Four drive units were necessary to move the two joints  $\varphi_1$  and  $\varphi_2$  at the endoscope tip. The endoscope had an outer diameter

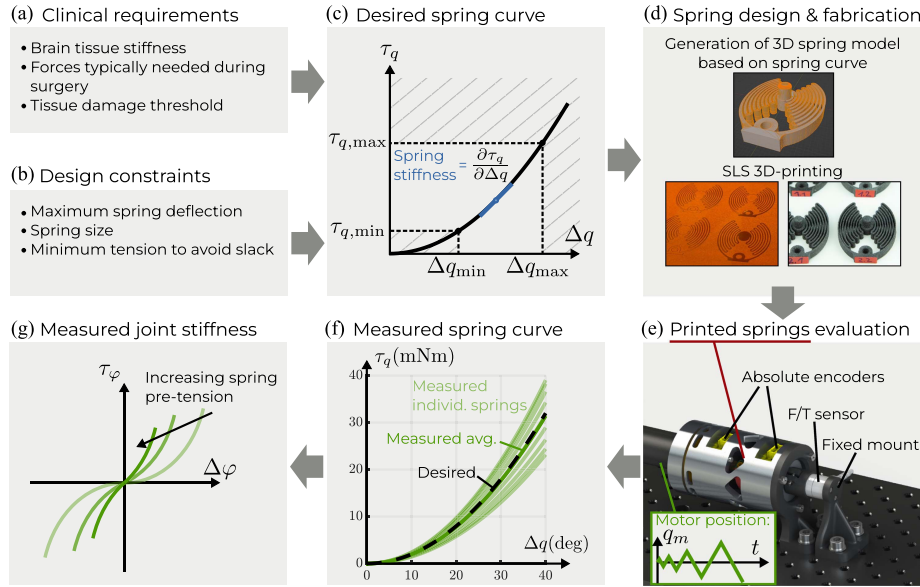


**Fig. 3.** Spring design and evaluation process. (a) Clinical requirements and (b) design constraints influence the specifications for the (c) desired spring curve, i.e., the relation between spring torque  $\tau_q$  and spring deflection  $\Delta q$ . (d) Design of the spring was then generated (as seen in CAD rendering) based on the desired spring curve, and the springs were 3D-printed with a selective laser sintering printer out of polyamide 12 (PA12). (e) CAD rendering of spring evaluation setup: A dc motor was commanded to deflect each spring to increasing deflection angles. On the load side, the spring was connected to a fixed mount with a force/torque sensor in between. Two rotational absolute encoders were used to measure the spring deflection. (f) Comparison of the quadratic fit of the measured data with the desired spring curve. (g) After integrating the springs into the antagonistic endoscope joint actuation, the joint stiffness could be varied by varying the pretension on both antagonistic springs.

of 7 mm, a similar size as currently used neuroendoscopy systems (Karl Storz LOTTA System:  $\varnothing 6.1$  mm,<sup>1</sup> B. Braun AESCULAP MINOP Trocar:  $\varnothing 6$  mm,<sup>2</sup> adeor Zeppelin Neuroscope:  $\varnothing 6.5$  mm).<sup>3</sup> The rigid links of the endoscope tip were 3-D printed with a stereolithography 3-D printer (Form 3 printer with Clear resin, Formlabs, Somerville, MA, USA). For reduced friction, the revolute joints were realized with miniature ball bearings (MPS Micro Precision Systems AG, Biel, Switzerland). The tendons actuating the second joint  $\varphi_2$  were routed around a pulley concentric with the first joint to ensure a constant lever arm.

Instead of connecting the output of the motors to the tendons with a rigid axis, we deliberately placed elastic elements in between because the human finger tendon–muscle transmission also has considerable elasticity. The exact mechanical behavior of this biological actuation and transmission system depends on many parameters [33]. Modeling approaches usually work with the assumption that the stiffness of a muscle–tendon compound increases with increasing force on the muscles [50], i.e., the biological elasticity cannot simply be modeled by a linear mechanical spring. Instead, a nonlinear, progressive stress-strain curve is needed to imitate the elastic behavior of the muscles and tendons [39], [51]. When arranged in an antagonistic setting to actuate a joint, this nonlinear elastic property enables to vary the stiffness of the joint by varying the co-contraction force (i.e., the pretension) on the muscles [32], [51]. Since we aimed to realize variable stiffness robotic endoscope joints, we included a custom-made rotational spring with a nonlinear

torque-deflection curve in our actuation. Two encoders (AMT23 14-bit absolute encoders, CUI Devices, Lake Oswego, OR, USA)—one on the motor side and one after the spring on the load side—were used to measure the deflection of the spring. Analogously, the neuromuscular system receives feedback on the state of its muscles and tendons from three main proprioceptors [52]: *muscle spindles*, *golgi tendon organs*, and *joint receptors*. We opted for minimal design complexity and did not incorporate three different types of sensors but instead solely relied on feedback from the two rotational encoders. Consequently, the torque information depended on an accurate model of the torque-deflection curve of the custom-made springs. The development process of our 3D-printed nonlinear springs is summarized in Fig. 3 and explained in more detail in the Supplementary Material. By evaluating the torque-deflection curve of the springs, we found that our spring design was suitable for printing progressive springs with a quadratic curve. The fitted quadratic coefficients used in (1) ranged from  $1.5 \cdot 10^{-2}$  mN · m/deg<sup>2</sup> to  $2.4 \cdot 10^{-2}$  mN · m/deg<sup>2</sup>. The mean fitted quadratic coefficient, at  $1.96 \cdot 10^{-2}$  mN · m/deg<sup>2</sup>, was close to the desired value of  $2 \cdot 10^{-2}$  mN · m/deg<sup>2</sup>, although the springs were spread with a relative error of up to 28%. The standard error of the regression remained below 0.03 mN · m/deg<sup>2</sup> for all nine printed springs [see Fig. 3(f)]. This regression served to calibrate the spring model used in the system control.

## B. Modeling and Control

A cascaded architecture was used to control the robotic endoscope (see Fig. 4), similarly to how we previously controlled a single robotic endoscope joint with series elastic actuation [29]. In an inner loop and for each of the four tendons, a PID controller

<sup>1</sup>[Online]. Available: <https://www.karlstorz.com/us/en/neurosurgery.htm>

<sup>2</sup>[Online]. Available: <https://www.bbraun.com/en/products/b0/minop.html>

<sup>3</sup>[Online]. Available: <https://www.adeor.com/de/download/>

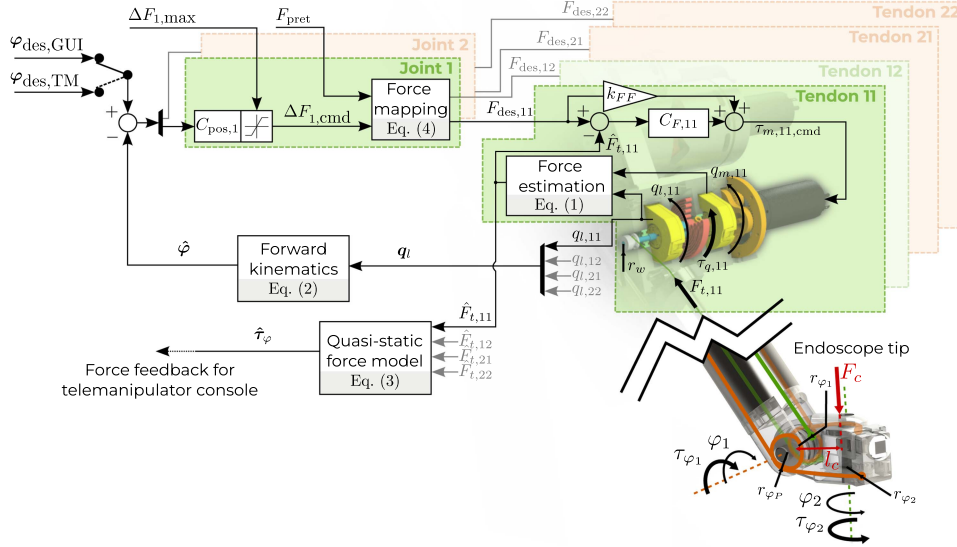


**Fig. 4.** Schematic of the robotic endoscope control and parameters of the kinematic model. The colors orange and green are used to distinguish between the controls of the first and second joints. The tendon force was controlled for every individual tendon in a separate inner tendon force control loop with controller  $C_{F,ij}$  and an additional feedforward term. As an example, the control loop  $C_{F,11}$  of the first joint ( $i = 1$ ) for the agonist tendon ( $j = 1$ ) is shown. In an outer loop, the endoscope tip position was controlled with a position controller  $C_{pos}$ . The threshold  $\Delta F_{i,max}$  could be set by the user to limit the maximal exerted endoscope joint torque (i.e., as a safety measure). If set to zero, the position controller was disabled, and the system was in a zero-torque control mode. The tendon pretension  $F_{pret}$  could be changed by the user to vary the stiffness of the endoscope tip joints. The desired position inputs for joint positions  $\varphi_1$  and  $\varphi_2$  came from a Graphical User Interface input ( $\varphi_{des,GUI}$ ) or from a telemanipulation console ( $\varphi_{des,TM}$ ). Force feedback to the user was possible by mapping the estimated joint torques  $\hat{\tau}_\varphi$  to rendered forces on the telemanipulation console.

$C_{F,ij}$  (controller gains:  $k_P = 18$ ,  $k_I = 240$ ,  $k_D = 0.12$ ) with feedforward term (with gain  $k_{FF} = 1$ ) minimized the error between a desired force on the tendons and an estimated tendon force feedback by commanding a torque  $\tau_{m,ij,cmd}$  at 1 kHz to the motor drives (MAXPOS 50/5, Maxon Motor AG, Sachseln, Switzerland), which controlled the motors in torque control mode [28]. A quadratic spring model  $\tau_q = c_s \cdot (\Delta q)^2$  was used to estimate the torque on the spring  $\tau_{q,ij}$ , and therefore the force on the tendon  $F_{t,ij}$ :

$$F_{t,ij} = \frac{\tau_{q,ij}}{r_w} = \frac{1}{r_w} c_{s,ij} (q_{m,ij} - q_{l,ij})^2 \quad (1)$$

where  $q_m$  is the rotational encoder position on the motor side of the spring and  $q_l$  the one on the load side. The combination of subscripts  $i \in \{1, 2\}$  (proximal or distal endoscope joint) and  $j \in \{1, 2\}$  (agonist or antagonist tendon) is used to uniquely denote the four tendon drive trains. The values for the quadratic coefficient of each spring  $c_{s,ij}$  were obtained with prior calibration (see Section II-A).

Pulling on agonist or antagonist tendons resulted in a torque around the endoscope joint to move the endoscope tip. An estimate  $\hat{\varphi} = \begin{pmatrix} \hat{\varphi}_1 \\ \hat{\varphi}_2 \end{pmatrix}$  of the current joint positions was computed with a forward kinematics model, i.e., the relation between load-side encoder position and endoscope joint positions:  $\hat{\varphi} = \mathbf{J} q_l$ . The Jacobian was

$$\mathbf{J} = \frac{\partial \varphi}{\partial q_l} = \frac{r_w}{2} \begin{bmatrix} -\frac{1}{r_{\varphi_1}} & \frac{1}{r_{\varphi_1}} & 0 & 0 \\ -\frac{1}{r_{\varphi_1} r_{\varphi_2}} & \frac{1}{r_{\varphi_1} r_{\varphi_2}} & -\frac{1}{r_{\varphi_2}} & \frac{1}{r_{\varphi_2}} \end{bmatrix} \quad (2)$$

where  $r_w$  is the winch radius,  $r_{\varphi_1}$  and  $r_{\varphi_2}$  are the lever arms of the tendon attachments at the endoscope links, and  $r_P$  is the pulley radius. The state estimation further included an estimate of the endoscope joint torque. Under the assumption that the robotic endoscope undergoes only slow movements, inertial effects were neglected. Therefore, instead of using a full dynamics model, the relationship between endoscope joint torque  $\tau_\varphi$  and tendon force  $\mathbf{F}_t$  was estimated using a quasi-static approximation

$$\tau_\varphi = r_w (\mathbf{J}^T)^{-1} \mathbf{F}_t \quad (3)$$

where  $(\mathbf{J}^T)^{-1}$  is the pseudoinverse of the transposed Jacobian matrix.

The estimated joint positions  $\hat{\varphi}$  served as sensor feedback to close the outer position control loop, in which the PID controllers  $C_{pos,i}$  minimized the error for each joint individually. The desired endoscope joint position was either set with an input field in a Graphical User Interface (GUI) ( $\varphi_{des,GUI}$ ) or through telemanipulation ( $\varphi_{des,TM}$ ). The output of  $C_{pos,i}$  was a tendon force command, which could further be limited to a user-defined threshold  $\Delta F_{i,max}$  as proposed in [29]. The resulting command  $\Delta F_{i,cmd}$  was then mapped to a desired force on each of the agonist and antagonist tendons

$$\begin{pmatrix} F_{des,i1} \\ F_{des,i2} \end{pmatrix} = \begin{cases} \begin{pmatrix} F_{pret} \\ F_{pret} + \Delta F_{i,cmd} \end{pmatrix}, & \Delta F_{i,cmd} \geq 0 \\ \begin{pmatrix} F_{pret} \\ F_{pret} - \Delta F_{i,cmd} \end{pmatrix}, & \Delta F_{i,cmd} < 0 \end{cases} \quad (4)$$

where  $F_{pret}$  is the user-defined tendon pretension. We implemented the following two different control modes.

**Position control mode:** Endoscope joint position tracking with controller gains for  $C_{\text{pos},i}$  ( $k_P = 0.23$ ,  $k_I = 2.5$ ,  $k_D = 0.0008$ ) that were tuned in a similar way as previously reported with a linear-spring series elastic actuation endoscope [29].

**Zero torque control mode:** The threshold  $\Delta F_{i,\text{max}}$  was set to zero, i.e., the desired input to the force controllers  $C_{F,ij}$  equaled the desired pretension and no additional output from the position controller. This controller scheme aimed at bringing the effective joint torque to zero, i.e., “giving way” to external torques.

In both control modes, the pretension for each agonist–antagonist pair could be changed by the user, effectively varying the mechanical stiffness of the joint. Since the total joint dynamics include a response from both the mechanics (“passive stiffness”) and the control (“active stiffness”), we use the term “pseudopassive stiffness” to describe the first few milliseconds of the joint response. Although the joint is actively controlled, the control is not fast enough to react to the impact, and thus this initial response is dominated by the passive mechanics and not by the active control.

Two layers of safety functions were implemented on the software control level to avoid over-deflection of the springs, which occurred when the force  $F_{t,\text{dmg}} = F_t(\Delta q = 30 \text{ deg})$  was applied to one of the tendons. As a first measure, the output of  $C_{\text{pos}}$  was limited to  $0.8 \cdot F_{t,\text{dmg}}$ . Furthermore, if an external impact caused any tendon force to exceed  $F_{t,\text{dmg}}$ , a safety stop was triggered, and all torque commands to the motors were set to zero.

### C. System Evaluation

1) **Forward Kinematic Model Evaluation:** We evaluated the joint position estimates (see Section II-B) with an angle scale attached to the inside of a half-sphere aligned with the joint rotation axes [see Fig. 5(a)].

2) **Frequency Response:** To evaluate the system behavior across the frequency spectrum and to find the operating limits, the endoscope tip joint was commanded to follow a sinusoidal movement with an amplitude of 10 deg in different frequencies from 1–64 Hz: the frequencies were  $f(n) = 2^n \text{ Hz}$ , with  $n \in [0, 6]$  and in steps of  $\Delta n = 0.25$ . To ensure that our data exclusively consisted of steady-state behavior, the recording for each frequency was only started once the system had settled to the oscillation at the desired frequency input. The system response, i.e., the actual estimated joint position, was recorded and analyzed to obtain the magnitude and phase shift relative to the desired sine wave. This experiment was repeated for different tendon pretensions  $F_{\text{pret}} = \{0.5, 0.75, 1, 1.25, 1.5\} \text{ N}$ . The following characteristics were read from the resulting Bode plot.

- 1) Gain margin: The magnitude of the sine wave at the frequency where the phase shift reaches  $-180^\circ$ .
- 2) Phase margin: The difference between the phase shift and  $-180^\circ$  at the frequency where the magnitude crosses 0 dB.
- 3) Bandwidth: The frequency where the magnitude crosses  $-3 \text{ dB}$ .

3) **Joint Torque Measurement Evaluation:** The accuracy of the estimated joint torque was evaluated with a force/torque

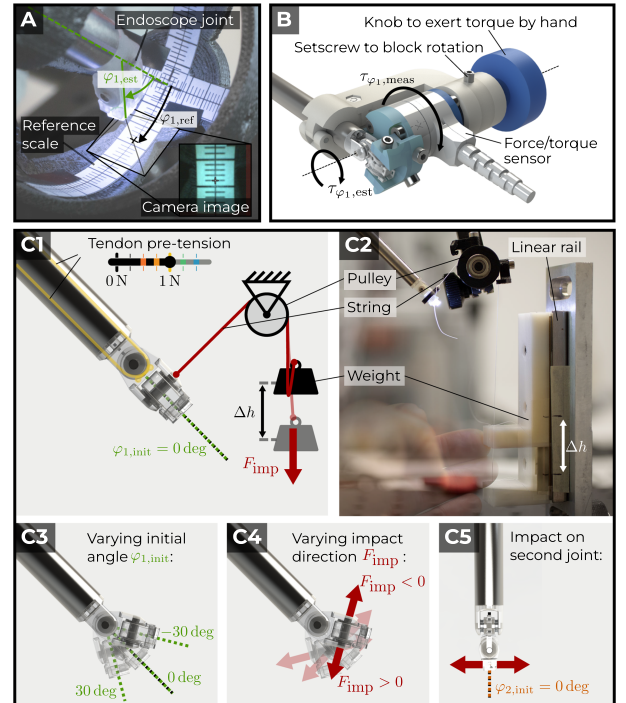


**Fig. 5.** Experiments overview. (a) Experimental setup to evaluate the kinematic model. The estimated joint position computed with the kinematics model  $\varphi_{1,\text{est}}$  was compared to the position to which the camera image center pointed on a reference scale  $\varphi_{1,\text{ref}}$ . One data point was recorded per two degrees on the scale from  $\varphi_{\text{ref}} = (-30, 30) \text{ deg}$  for both joints ( $n = 30$  per joint). The reference scale was rigidly attached to the endoscope shaft and aligned to the evaluated joint rotation axis. (b) Experimental setup to evaluate joint torque estimation. Light blue: part of the axis that rigidly connected the endoscope link to the force/torque sensor. Dark blue: part of the axis connected to the other side of the force/torque sensor and is either fixed with a setscrew or held by hand to exert an external torque. (c) Overview of joint impact experiments. (C1) and (C2) Experimental setup to exert an impact force on the endoscope link, which resulted in a torque around the endoscope joint. A weight in the form of a carriage was dropped from a defined height  $\Delta h$ . The weight was connected to the endoscope link through a string, which was routed over a pulley such that the force was applied to the endoscope link at a right angle. The impact (letting the weight fall) was repeated five times per tendon pretension. The behavior of the robot was sampled at different locations in the workspace by varying (C3) the initial angle, (C4) the impact direction, and (C5) the joint number.

sensor (Nano17-E F/T Sensor, ATI Industrial Automation, Apex, NC, USA) mounted concentrically to the endoscope tip joint [see Fig. 5(b)]. The joint torque was recorded for three different cases as follows.

- 1) Position control with external torque applied: The control mode was set to position control with the desired position set to  $0^\circ$ . Then, the axis was rotated by hand to exert torque on the endoscope joint.
- 2) Position control with internal torque applied: The control mode was set to position control, and the axis was locked against rotation with a setscrew to fix the joint in a straight configuration ( $0^\circ$ ). The endoscope joint was then commanded to move in a telemanipulated mode. Since the rotation was locked in this position, commands exerted torque on the force–torque sensor.

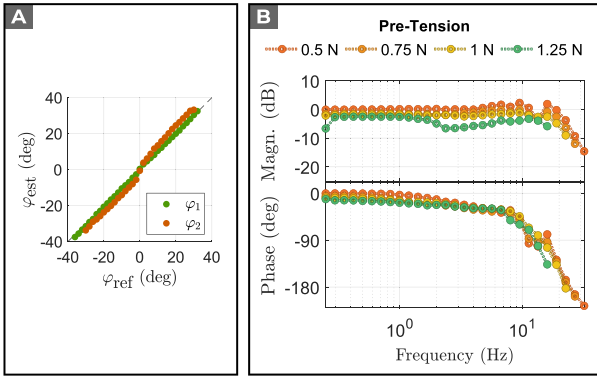


**Fig. 6.** (a) Results from evaluating the estimated endoscope joint position. (b) Bode plot: Frequency analysis of the system at different tendon pre-tensions. Filled markers denote that the maximum spring deflection force threshold  $F_t = 0.8 F_{t,\text{dmg}}$  was reached (see Section II-B). The run with  $F_{\text{pret}} = 1.25 \text{ N}$  (green) could not be completed since the safety stop ( $F_t = F_{t,\text{dmg}}$ ) was triggered at higher frequencies. With  $F_{\text{pret}} = 1.5 \text{ N}$ , position control failed, and the desired sine wave could not be followed.

- 3) Zero torque control: The endoscope was controlled in zero torque control mode, and the joint was moved by rotating the axis by hand.

The joint torque estimated with spring deflection and the forward kinematics was compared against the torque in  $z$ -direction measured with the force/torque sensor. This experiment was repeated for five different tendon pretensions: 0.5 N, 0.75 N, 1 N, 1.25 N, and 1.5 N. Furthermore, the experiment was performed for both joints:  $\varphi_1$  and  $\varphi_2$ . Data was recorded for each of these cases for 15 s.

**4) Impact Response:** We evaluated whether a stiffness variation of the robotic endoscope joints is possible and whether that stiffness variation affects the system response to an external impact. A weight was attached to one of the rigid links of the endoscope tip with a string [see Fig. 5(c)]. By letting the weight fall from a defined height of  $\Delta h = 2 \text{ cm}$ , an impact force  $F_{\text{imp}}$  was exerted on the link, which resulted in a torque around the endoscope joint. The string was routed over a pulley to ensure the force direction was orthogonal to the joint's rotational axis in the initial position. To attach the string to the endoscope, a 3D-printed holder was clipped on the endoscope link. The experiment was performed for different initial positions ( $-30^\circ$ ,  $0^\circ$ ,  $30^\circ$ ) as well as for an impact in both directions to sample the system behavior at different locations in its workspace. For each of the variations, the system response was recorded for five impacts with five different tendon pre-tensions 0.5 N, 0.75 N, 1 N, 1.25 N, and 1.5 N in both position control and zero torque control mode.

### III. RESULTS

#### A. Forward Kinematic Model Evaluation

The maximum absolute error between the estimated joint position and the reference position was  $1.5^\circ$  for  $\varphi_1$  (mean error  $0.3^\circ$ , std  $0.68^\circ$ ), and  $4.7^\circ$  for  $\varphi_2$  [mean error  $0.02^\circ$ , std  $3.8^\circ$ , see Fig. 6(a)].

**TABLE I**  
RESULTS OF GENERALIZED LINEAR MODEL REGRESSION FOR JOINT 1 STIFFNESS

$F_{\text{pret}}$	Model stiffness	Measured stiffness	Rel. error
0.5 N	0.25 mN·m/deg	0.40 mN·m/deg	62 %
1 N	0.35 mN·m/deg	0.53 mN·m/deg	52 %
1.5 N	0.42 mN·m/deg	0.63 mN·m/deg	48 %

#### B. Frequency Response

The system's response to excitation at different sine frequencies is shown in a Bode plot [see Fig. 6(b)]. Accurate and stable position control was achieved up to a tendon pretension of 1 N. Above 1 N pretension on the tendons, the joint could no longer follow a proper sine wave. For pretensions up to 1 N, the bandwidth was larger than 13.1 Hz. Both the gain margin and the phase margin were positive and sufficiently large to assume system stability. For all pretensions 0.5 N through 1 N, the magnitude of the system response peaked at 16 Hz, indicating a resonance around this frequency. For all tendon pretensions, the maximum tendon force threshold was reached [denoted by a filled circle in Fig. 6(b)] for frequencies around resonance. Detailed results can be found in the Supplementary Material (see Table III).

#### C. Joint Torque Evaluation Results

The comparison between estimated and measured torque can be seen in Fig. 7. Considering the data from all pretensions and control modes, the mean absolute error between estimated and measured torque was  $1.3 \text{ mN} \cdot \text{m}$  (max.  $5.2 \text{ mN} \cdot \text{m}$ ) for joint 1 and  $1.7 \text{ mNm}$  (max.  $8.0 \text{ mNm}$ ) for joint 2. There was a tendency toward lower errors for torque applied by telemanipulation (“PosC – int.”) compared to torque applied externally (“PosC – ext.” and “ZeroTC – ext.”). However, no tendency was observed for the relation between error and tendon pretension.

#### D. Impact Response

The system response to an impact is shown in Fig. 8 for an impact on joint 1, with an initial joint position of  $0^\circ$ , and in negative joint direction. The external force after an impact ( $t = 0\text{s}$ ) caused the joint to deflect from its initial position. In position control mode, the joint ultimately settled again close to its initial position, while it stayed in a deflected position in zero torque control mode. The maximal joint torques estimated by spring deflection did not vary significantly for different tendon pretensions. When plotting the joint torque against joint deflection immediately after the impact, the slope of the curve increased with increasing tendon pretension. Similar results were obtained when starting from a different initial joint position and when the impact force was applied from a different direction. The results of a regression to fit every tested pretension on the tendons actuating the first joint  $\varphi_1$  to an experimentally determined joint stiffness, and the comparison to the theoretical stiffness can be seen in Table I.

However, the response of the second endoscope tip joint  $\varphi_2$  to impacts was not as largely affected by the tendon pretension

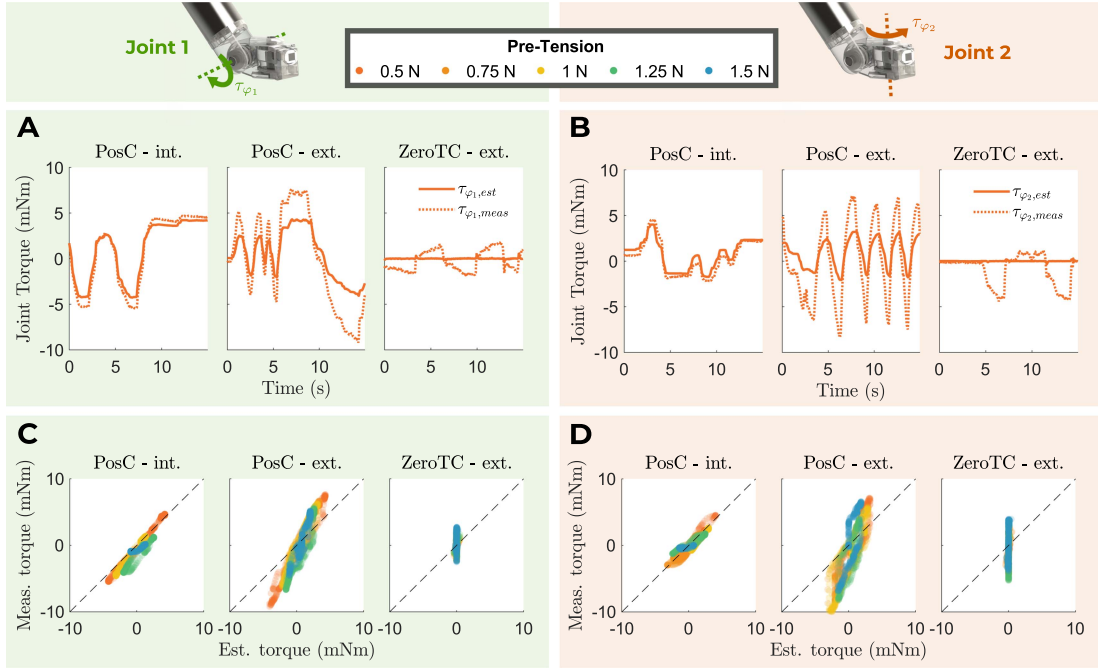


**Fig. 7.** Joint torque estimate evaluation results. (a) Estimated joint 1 torque  $\tau_{\varphi_1,\text{est}}$  was compared to the torque  $\tau_{\varphi_1,\text{meas}}$  measured with a force / torque sensor over time. (b) Analogous for joint 2. (c) Measured torque  $\tau_{\varphi_1,\text{meas}}$  was plotted against the estimated torque  $\tau_{\varphi_1,\text{est}}$ . In an ideal case, the estimated torque would be identical to the measured one, which is represented by the diagonal black dashed line. (d) Analogous for joint 2. PosC-int. = torque commanded by telemanipulation (internally) while the output axis was fixed. PosC-ext. = torque applied externally and in position control. ZeroTC-ext. = torque applied externally and in zero torque control.

as for  $\varphi_1$ . No relevant difference in stiffness of  $\varphi_2$  could be observed for different pretensions.

#### IV. DISCUSSION

By evaluating the forward kinematics model, we showed that reliable position control is possible for an endoscope tip driven by antagonistic series elastic actuators. However, we only evaluated the error on the two main rotational axes of the endoscope (i.e., always keeping one joint at zero). Thus, we did not evaluate the error over the complete workspace of the endoscope tip. While position control was accurate with low pretensions, following a position demand became increasingly difficult above 1.25 N. The same decrease in control performance with increasing tendon pre-tension was visible when evaluating the system's frequency response. Only pretensions up to 1 N resulted in sufficient gain margins, phase margins, and control bandwidth to fulfill the control requirements expected for brain surgeries; pretensions above 1 N did not. These findings go against the paradigm that a stiffer actuation leads to more torque-tracking bandwidth. However, we attribute this loss in bandwidth not to the joint stiffness increase but rather to the fact that more pretension leads to less further admissible deflection of the spring, thus less admissible torque that could be exerted on the endoscope joint to move to the desired position. Two modifications could improve this: first, using springs with a larger quadratic coefficient, which would, however, limit the sensitivity of the force measurement. Second, implementing a mechanical limit for the deflection of the spring to render the transmission

“rigid” and allow higher torques than what the spring could withstand. This limit would, however, introduce a discontinuity in the spring curve. Furthermore, when the mechanical limit is reached, the exact torque output cannot be estimated through spring deflection.

The joint torque measurements seemed accurate, considering that the sensors were placed outside the endoscope and that friction and other transmission nonlinearities were included in the measurements. Interestingly, there was no correlation between tendon pretension and torque measurement error. These results indicate that in our tested range of stiffnesses, the friction and tendon elasticity had a larger limiting effect on the torque-measuring sensitivity than the resolution of the encoders.

These nonlinear transmission effects were also visible when evaluating the impact response of the system. Although both joints showed some passive compliance, which helps to decrease the contact force peaks, varying the stiffness did not work for both joints. While the stiffness could be controlled for joint 1, we could not achieve a varying stiffness for joint 2. We assume that the longer motion transmission for joint 2 absorbed a large part of the impact energy through friction, tendon elongation, and deformation of the endoscope shaft instead of the impact being fully transmitted to the springs and the resulting torque being detected via spring deflection. All these transmission effects also increased the measured torque on joint 1 and resulted in a higher measured stiffness than the modeled one. Decreasing the friction of the transmission and ensuring that a bigger part of the impact energy reaches the springs could potentially resolve the issue. However, no matter how well the endoscope tip is designed and

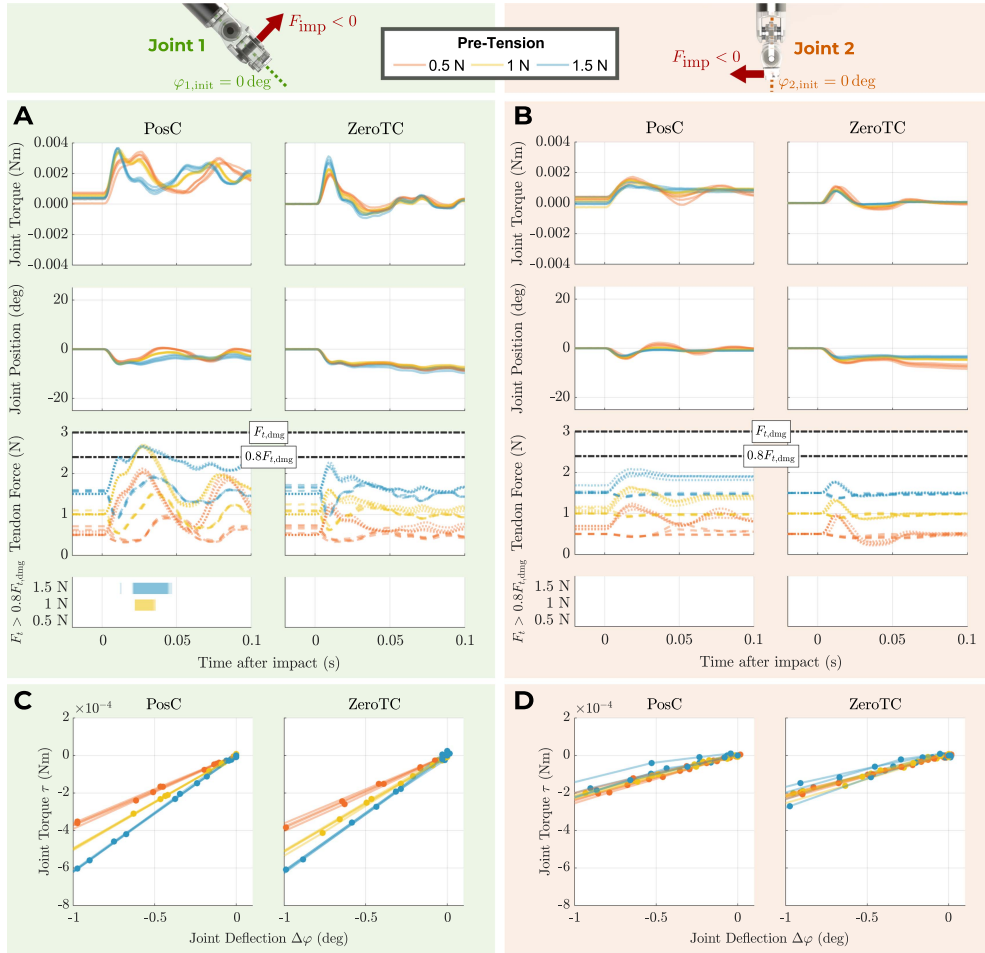


**Fig. 8.** Representative plots of the system response after an impact to the endoscope tip. (a) Impact was directed such that a torque was exerted on joint 1 with an initial position of  $\varphi_{1,\text{init}} = 0^\circ$  and in negative joint direction. All plotted values are based on the rotational encoder measurements and then converted using forward kinematics (joint position) and the quasi-static force model (joint torque and tendon force). To visualize the antagonistic principle, the third row shows the estimated tendon force on both the agonist (dashed line) and the antagonist (dotted line). The bottom row indicates whether the tendon force safety limit  $F_t = 0.8F_{t,\text{dmg}}$  was exceeded. (b) Impact was directed such that a torque was exerted on joint 2 with an initial position of  $\varphi_{2,\text{init}} = 0^\circ$  and in negative joint direction. (c) When plotting the joint torque versus joint deflection and zooming in on the first milliseconds after impact (i.e., joint deflection  $|\Delta\varphi| < 1^\circ$ ), the pseudopassive response of the joint to an impact can be seen. For joint 1, there is a clear increase in stiffness for increasing pretension, which can be observed by the steeper slope of the torque-deflection curve. (d) No change in stiffness can be seen for different pretensions for joint 2.

manufactured, there will always remain some residual friction in the transmission. Thus, future work could investigate the possibility of compensating for these transmission effects with a model or how to design tendon transmissions to stack many joints in series such that sensitive position control of the joints is still possible by controlling the force on the antagonistic tendons. Summing up, with our approach of combining antagonistic series elastic actuation with discrete joints, we achieved the following.

- 1) Mechanical compliance and, therefore, compensation of force peaks and faster reaction to impacts than by closed-loop control of stiff actuation.
- 2) Extrinsic endoscope joint torque sensing can be used for haptic feedback and force control.
- 3) Precise joint position measurement and, therefore, accurate robot shape estimation due to deterministic behavior. This leads to observability and controllability of the entire structure on the joint level, which can be used to apply

conventional forward and inverse kinematics, as well as path planning for preoperative planning.

- 4) A variable passive stiffness of the first joint that may lead to lower reflected inertia on impacts, but did with the current design not improve positioning accuracy or bandwidth. Further research needs to investigate the passive stiffness range required for ventricular endoscopy tasks and whether our achieved stiffness accuracy is sufficient.

Even though brain surgery is an evident application of our technology, it could easily be extended to other surgical disciplines. For example, tendon-driven laparoscopy robots, such as the popular da Vinci surgical system could be actuated with SEA-based drive units to make their distal joints torque-controlled. By adjusting the spring curve, the higher required forces in other surgical disciplines could be achieved. Furthermore, potential applications extend beyond simply providing a safety mechanism for joints used for endoscope camera movement, but robotic endoscopes based on antagonistic SEA could

greatly improve tissue manipulation tasks: giving haptic feedback on tissue dissection, measuring gripping forces, receiving information on tissue stiffness.

## V. CONCLUSION

In this article, we realized a bio-inspired actuation concept for tendon-driven robots used in minimally invasive surgery, combining the advantages of antagonistic series elastic actuation with those of discrete joints. With a set of experiments, we showed that the system can be mechanically compliant against impact forces while at the same time achieving reliable joint positioning and delivering contact force information. Compared to standard stiff neuroendoscopes, our proposed robotic actuation would offer increased degrees of freedom and the capability to access the entire ventricular system through one burr hole while directly addressing the safety risks from the additional degrees of freedom: Controlling the torque at the endoscope joint level facilitates staying below damage thresholds to reduce tissue injury.

## ACKNOWLEDGMENT

The authors would like to thank Sascha Martin and his team at the mechanical workshop of the Physics Department at the University of Basel for their help with manufacturing the actuation unit of our system. The authors would also like to thank Florian Thieringer, Neha Sharma, Michel Beyer, Andreas Roser, Michaela Maintz, and Jokin Zubizarreta-Oteiza of the Swiss-MAM group, University of Basel for 3D-printing the endoscope tip links that we received.

## REFERENCES

- [1] A. Grotenhuis, "Neuroendoscopic instruments and surgical technique," in *Neuroendoscopy*. Berlin, Germany: Springer, 2013, pp. 81–91.
- [2] M. G. Yaşargil and S. I. Abdulrauf, "Surgery of intraventricular tumors," *Neurosurgery*, vol. 62, no. 6, pp. SHC1029–SHC1041, Jun. 2008.
- [3] K. W. Li, C. Nelson, I. Suk, and G. I. Jallo, "Neuroendoscopy: Past, present, and future," *Neurosurgery Focus*, vol. 19, no. 6, pp. 1–5, Dec. 2005.
- [4] F. Ebel, L. Greuter, L. Mariani, R. Guzman, and J. Soleman, "Intracranial neuroendoscopy in children and adults: Where do the differences lie?," *World Neurosurgery*, vol. 177, pp. e94–e109, Jun. 2023.
- [5] J. Roth and S. Constantini, "Combined rigid and flexible endoscopy for tumors in the posterior third ventricle," *J. Neurosurg.*, vol. 122, no. 6, pp. 1341–1346, Jun. 2015.
- [6] J. Soleman and R. Guzman, "Neurocognitive complications after ventricular neuroendoscopy: A systematic review," *Behav. Neurol.*, vol. 2020, pp. 1–13, Mar. 2020.
- [7] K. Price et al., "Using robotics to move a neurosurgeon's hands to the tip of their endoscope," *Sci. Robot.*, vol. 8, no. 82, Sep. 2023, Art. no. eadg6042.
- [8] M. F. Rox et al., "Mechatronic design of a two-arm concentric tube robot system for rigid neuroendoscopy," *IEEE/ASME Trans. Mechatron.*, vol. 25, no. 3, pp. 1432–1443, Jun. 2020.
- [9] Y. Gao, K. Takagi, T. Kato, N. Shono, and N. Hata, "Continuum robot with follow-the-leader motion for endoscopic third ventriculostomy and tumor biopsy," *IEEE Trans. Biomed. Eng.*, vol. 67, no. 2, pp. 379–390, Feb. 2020.
- [10] H. Takasuna et al., "Use of a micromanipulator system (NeuRobot) in endoscopic neurosurgery," *J. Clin. Neurosci.*, vol. 19, no. 11, pp. 1553–1557, Nov. 2012.
- [11] C. S. Karas and E. A. Chiocca, "Neurosurgical robotics: A review of brain and spine applications," *J. Robot. Surg.*, vol. 1, no. 1, pp. 39–43, Feb. 2007.
- [12] R. Elsabeh, S. Singh, J. Shasho, Y. Saltzman, and J. M. Abrahams, "Cranial neurosurgical robotics," *Brit. J. Neurosurgery*, vol. 35, no. 5, pp. 532–540, Aug. 2021.
- [13] G. Tholey, J. P. Desai, and A. E. Castellanos, "Force feedback plays a significant role in minimally invasive surgery," *Ann. Surg.*, vol. 241, no. 1, pp. 102–109, Jan. 2005.
- [14] Y. Uchida et al., "Robotic instruments outside the surgical field can cause problems: A case of critical bleeding during robotic distal pancreatectomy," *Asian J. Endoscopic Surg.*, vol. 16, no. 3, pp. 588–590, May 2023.
- [15] U. Seibold, B. Kubler, and G. Hirzinger, "Prototype of instrument for minimally invasive surgery with 6-axis force sensing capability," in *Proc. 2005 IEEE Int. Conf. Robot. Autom.*, 2005, pp. 496–501.
- [16] H.-R. Choi, D.-H. Lee, U. Kim, T. Gulrez, W. J. Yoon, and B. Hannaford, "A laparoscopic grasping tool with force sensing capability," *IEEE/ASME Trans. Mechatron.*, vol. 21, no. 1, pp. 130–141, Feb. 2016.
- [17] E. Tagliabue, D. Meli, D. DallAlba, and P. Fiorini, "Deliberation in Autonomous Robotic Surgery: A Framework for Handling Anatomical Uncertainty," in *Proc. 2022 Int. Conf. Robot. Autom.*, 2022, pp. 11080–11086.
- [18] A. L. Trejos, R. V. Patel, and M. D. Naish, "Force sensing and its application in minimally invasive surgery and therapy: A survey," *Proc. Inst. Mech. Eng. C*, vol. 224, no. 7, pp. 1435–1454, Jan. 2010.
- [19] H. Sang, J. Yun, R. Monfaredi, E. Wilson, H. Fooladi, and K. Cleary, "External force estimation and implementation in robotically assisted minimally invasive surgery," *Int. J. Med. Robot. Comput. Assist. Surg.*, vol. 13, no. 2, May 2017, Art. no. e1824.
- [20] M. B. Schäfer, J. G. Meiringer, J. Nawratil, L. Worbs, G. A. Giacoppo, and P. P. Pott, "Estimating gripping forces during robot-assisted surgery based on motor current," *Curr. Directions Biomed. Eng.*, vol. 8, no. 1, pp. 105–108, Jul. 2022.
- [21] C. Francis, T. Sato, T. Okuyama, and M. Tanaka, "A cable driven robotic palpation system with contact force sensing based on cable tension observation," *Int. J. Med. Robot. Comput. Assist. Surg.*, vol. 18, no. 6, Jul. 2022, Art. no. e2435.
- [22] M. Haghhighipanah, M. Miyasaka, and B. Hannaford, "Utilizing elasticity of cable-driven surgical robot to estimate cable tension and external force," *IEEE Robot. Autom. Lett.*, vol. 2, no. 3, pp. 1593–1600, Jul. 2017.
- [23] A. Bicchi and G. Tonietti, "Fast and "soft-arm" tactics," *IEEE Robot. Autom. Mag.*, vol. 11, no. 2, pp. 22–33, Jun. 2004.
- [24] G. A. Pratt and M. M. Williamson, "Series elastic actuators," in *Proc. 1995 IEEE/RSJ Int. Conf. Intell. Robot. Syst.*, Pittsburgh, PA, USA, 1995, vol. 1, pp. 399–406.
- [25] X. Zhou and S. Bi, "A survey of bio-inspired compliant legged robot designs," *Bioinspiration Biomimetics*, vol. 7, no. 4, Nov. 2012, Art. no. 041001.
- [26] P. Agarwal and A. D. Deshpande, "Series elastic actuators for small-scale robotic applications," *J. Mechanisms Robot.*, vol. 9, no. 3, Mar. 2017, Art. no. 031016.
- [27] Y. Zimmermann, M. Sommerhalder, P. Wolf, R. Riener, and M. Hutter, "ANYExo 2.0: A fully actuated upper-limb exoskeleton for manipulation and joint-oriented training in all stages of rehabilitation," *IEEE Trans. Robot.*, vol. 39, no. 3, pp. 2131–2150, Jun. 2023.
- [28] L. Fasel, N. Gerig, P. C. Cattin, and G. Rauter, "Tendon force control evaluation for an endoscope with series elastic actuation," in *New Trends in Medical and Service Robotics*. Berlin, Germany, 2020, pp. 118–126.
- [29] L. Fasel, N. Gerig, P. C. Cattin, and G. Rauter, "The SEA-scope: Torque-limited endoscopic joint control for telemanipulation or visual servoing through tendon force control with series elastic actuation," in *Proc. 2021 Symp. Med. Robot.*, 2021, pp. 1–7.
- [30] L. Fasel, N. Gerig, P. C. Cattin, and G. Rauter, "Control evaluation of antagonistic series elastic actuation for a robotic endoscope joint," *J. Bionic Eng.*, vol. 19, no. 4, pp. 965–974, Mar. 2022.
- [31] J. Pratt, B. Krupp, and C. Morse, "Series elastic actuators for high fidelity force control," *Ind. Robot. Int. J.*, vol. 29, no. 3, pp. 234–241, Jun. 2002.
- [32] S. Wolf et al., "Variable stiffness actuators: Review on design and components," *IEEE/ASME Trans. Mechatron.*, vol. 21, no. 5, pp. 2418–2430, Oct. 2016.
- [33] N. Hogan, "Adaptive control of mechanical impedance by coactivation of antagonist muscles," *IEEE Trans. Autom. Control*, vol. 29, no. 8, pp. 681–690, Aug. 1984.
- [34] S. Migliore, E. Brown, and S. DeWeerth, "Biologically inspired joint stiffness control," in *Proc. 2005 IEEE Int. Conf. Robot. Autom.*, 2005, pp. 4508–4513.
- [35] W. G. Darling and K. J. Cole, "Muscle activation patterns and kinetics of human index finger movements," *J. Neurophysiol.*, vol. 63, no. 5, pp. 1098–1108, May 1990.

- [36] E. Burdet, R. Osu, D. W. Franklin, T. E. Milner, and M. Kawato, "The central nervous system stabilizes unstable dynamics by learning optimal impedance," *Nature*, vol. 414, no. 6862, pp. 446–449, Nov. 2001.
- [37] K. Akazawa, T. E. Milner, and R. B. Stein, "Modulation of reflex EMG and stiffness in response to stretch of human finger muscle," *J. Neurophysiol.*, vol. 49, no. 1, pp. 16–27, Jan. 1983.
- [38] B. Vanderborght et al., "Variable impedance actuators: A review," *Robot. Auton. Syst.*, vol. 61, no. 12, pp. 1601–1614, Dec. 2013.
- [39] R. Ham, T. Sugar, B. Vanderborght, K. Hollander, and D. Lefebvre, "Compliant actuator designs," *IEEE Robot. Autom. Mag.*, vol. 16, no. 3, pp. 81–94, Sep. 2009.
- [40] G. Grioli et al., "Variable stiffness actuators: The user's point of view," *Int. J. Robot. Res.*, vol. 34, no. 6, pp. 727–743, Mar. 2015.
- [41] B. Vanderborght et al., "Variable impedance actuators: Moving the robots of tomorrow," in *Proc. 2012 IEEE/RSJ Int. Conf. Intell. Robot. Syst.*, 2012, pp. 5454–5455.
- [42] B. Vanderborght, R. V. Ham, B. Verrelst, M. V. Damme, and D. Lefebvre, "Overview of the Lucy project: Dynamic stabilization of a biped powered by pneumatic artificial muscles," *Adv. Robot.*, vol. 22, no. 10, pp. 1027–1051, Jan. 2008.
- [43] L. Liu, S. Leonhardt, C. Ngo, and B. J. E. Misgeld, "Impedance-controlled variable stiffness actuator for lower limb robot applications," *IEEE Trans. Automat. Sci. Eng.*, vol. 17, no. 2, pp. 991–1004, Apr. 2020.
- [44] V. Grosu, C. Rodriguez-Guerrero, S. Grosu, B. Vanderborght, and D. Lefebvre, "Design of smart modular variable stiffness actuators for robotic-assistive devices," *IEEE/ASME Trans. Mechatron.*, vol. 22, no. 4, pp. 1777–1785, Aug. 2017.
- [45] E. Barrett, M. Reiling, G. Barbieri, M. Fumagalli, and R. Carloni, "Mechatronic design of a variable stiffness robotic arm," in *Proc. 2017 IEEE/RSJ Int. Conf. Intell. Robot. Syst.*, 2017, pp. 4582–4588.
- [46] C. Chautems, A. Tonazzini, Q. Boehler, S. H. Jeong, D. Floreano, and B. J. Nelson, "Magnetic continuum device with variable stiffness for minimally invasive surgery," *Adv. Intell. Syst.*, vol. 2, no. 6, Oct. 2019, Art. no. 1900086.
- [47] L. Blanc, A. Delchambre, and P. Lambert, "Flexible medical devices: Review of controllable stiffness solutions," *Actuators*, vol. 6, no. 3, Jul. 2017, Art. no. 23.
- [48] A. Loeve, P. Breedveld, and J. Dankelman, "Scopes too flexible...and too stiff," *IEEE Pulse*, vol. 1, no. 3, pp. 26–41, Nov./Dec. 2010.
- [49] X. Gu and H. Ren, "A survey of transoral robotic mechanisms: Distal dexterity, variable stiffness, and triangulation," *Cyborg Bionic Syst.*, vol. 4, Jan. 2023, Art. no. 0007.
- [50] K. L. Jakubowski, D. Ludvig, D. Bujnowski, S. S. M. Lee, and E. J. Perreault, "Simultaneous quantification of ankle, muscle, and tendon impedance in humans," *IEEE Trans. Biomed. Eng.*, vol. 69, no. 12, pp. 3657–3666, Dec. 2022.
- [51] C. E. English and D. Russell, "Mechanics and stiffness limitations of a variable stiffness actuator for use in prosthetic limbs," *Mech. Mach. Theory*, vol. 34, no. 1, pp. 7–25, 1999. [Online]. Available: <https://www.sciencedirect.com/science/article/pii/S0094114X98000263>
- [52] J. C. Tuthill and E. Azim, "Proprioception," *Curr. Biol.*, vol. 28, no. 5, pp. R194–R203, Mar. 2018.

**Lorin Fasel** received the B.Sc. degree in mechanical engineering and the M.Sc. degree in robotics, systems, and control from ETH Zurich, Zurich, Switzerland, in 2015 and 2018, respectively.

He conducted his master's thesis on the actuation design of a bone-mounted parallel mechanism at the BIROMED-Lab, University of Basel, Basel, Switzerland, and in 2018, he joined the same lab as a Doctoral Candidate. His research focuses on the development of robotic endoscopes with series elastic actuation for surgical applications such as neurosurgery.

**Nicolas Gerig** (Member, IEEE) received the B.Sc. and M.Sc. degrees in mechanical engineering and the Ph.D. degree in robotics from ETH Zurich, Zurich, Switzerland, in 2010, 2013, and 2018, respectively.

In 2012, he joined the Florida Institute for Human and Machine Cognition, Pensacola, FL, USA, for his master's thesis on fall prevention of a robotic leg orthosis. In his Ph.D., he developed a virtual trainer for robot-assisted movement training. Since 2018, he has been the deputy-head of the BIROMED-Lab, Department of Biomedical Engineering, University of Basel, Basel, Switzerland. His current research focuses on developing novel robotic surgery platforms.

**Aschraf Danun** received the bachelor's and master's in mechanical engineering from TU Munich, Munich, Germany, in 2014 and 2017, respectively, and the Ph.D. from ETH Zurich, Zurich, Switzerland, in 2024.

He is an R&D Project Manager at Thermoplan AG, Switzerland. His doctoral research, conducted with the Product Development Group , ETH Zurich, Zurich, Switzerland. His research focuses on the design for additive manufacturing of compliant mechanisms, with a specific emphasis on potential applications in the medical and robotic fields.

**Mirko Meboldt** received the bachelor.s and master's degree in mechanical engineering and the Ph.D. degree in product development from the Karlsruhe Institute of Technology (KIT), Karlsruhe, Germany, in 2008.

Following a successful industrial career at Hilti AG, Schaan, Liechtenstein, he was appointed in 2012 as a Full Professor of product development and engineering design at ETH Zurich, Zurich, Switzerland. He leads the Product Development Group Zurich, focusing on design for emerging technologies, with a particular emphasis on additive manufacturing and the digital value chain.

**Raphael Guzman** completed medical school from the University of Bern, Bern, Switzerland, in 1998, and the neurosurgery board certification in 2007.

He was a Fellow with Stanford University, Stanford, CA, USA, and Hospital Necker, Paris, France. In 2011, he joined the University of Basel, Basel, Switzerland, where he is currently a Department Chair and Professor of neurosurgery and neurosciences, as well as Chief of cerebrovascular and pediatric neurosurgery. Next to clinical research, his research include advancing technologies, such as virtual and augmented reality and minimally invasive endoscopy for applications in neurosurgery.

**Philippe C. Cattin** received the B.Sc. degree in computer science from the University of Applied Sciences in Brugg/Windisch, Windisch, Switzerland, in 1991, and the M.Sc. degree in computer science and the Ph.D. degree in robotics from ETH Zurich, Zurich, Switzerland, in 1991 and 2003, respectively.

From 2003 to 2007, he was a Postdoctoral Fellow with the Computer Vision Laboratory, ETH Zurich. In 2007, he joined the University of Basel, Basel, Switzerland, as an Assistant Professor and was appointed to Full Professor in 2019. There, he founded the Center for Medical Image Analysis and Navigation and is heading the Department of Biomedical Engineering. His research interests include medical image analysis, image-guided therapy, robotics-guided laser osteotomy, and virtual reality.

**Georg Rauter**(Member, IEEE) received the first Diploma in mechanical modeling from MATMECA, Bordeaux, France, in 2006, and the second Diploma in mechanical engineering from TU-Graz, Austria, in 2008, and the Ph.D. degree in robotics from ETH Zurich, Zurich, Switzerland, in 2014.

From 2014 to 2016, he was a Postdoc with ETH Zurich, the University of Southern California, Los Angeles, CA, USA, and the University of Zurich, Zurich. In 2016, he joined the Department of Biomedical Engineering with the University of Basel, Basel, Switzerland, as an Assistant Professor. Since 2022, he holds a structural position as Associate Professor for surgical robotics with the University of Basel, and heads the Bio-Inspired Robots for Medicine Laboratory. His research interests include the development of complete robotic and mechatronic systems for enabling minimally invasive surgical procedures.